Distinct Brain-derived TDP-43 Strains from FTLD-TDP Subtypes Induce Diverse Morphological TDP-43 Aggregates and Spreading Patterns *in vitro* and *in vivo*.

Sílvia Porta[1*], Yan Xu[1], Tagan Lehr[1], Bin Zhang[1], Emily Meymand[1], Modupe Olufemi[1], Anna Stieber[1], Edward B. Lee[2], John Q. Trojanowski[1], Virginia M.-Y. Lee[1*]

Supplementary Methods

Supplementary Figures

Fig. S1 Differential neuropathological distribution of phosphorylated TDP-43 aggregates and biochemical analysis of sark-insoluble brain extracts from different FTDP-TDP subtypes used in this study

Fig. S2 Morphological differences of TDP-43 aggregates in iGFP-NLSm cells transduced with distinct FTLD-TDP subtypes are not associated with differences in cytotoxicity or cell viability

Fig. S3 Morphological features of TDP-43 aggregates induced in iGFP-NLSm cells are propagated from progenitor to offspring cells

Fig. S4 Differences in morphological features of TDP-43 aggregates are associated with distinct TDP-43 strains in different FTLD-TDP subtypes

Fig. S5 TDP-43 aggregates are phosphorylated at Ser409/Ser410 and Ser403/Ser404 residues and cytoplasmic hTDP-43_{NLSm} proteins entirely recruited into inclusions

Fig. S6 p409-410 positive NCIs co-localize with p62 and ubiquitin

Fig. S7 Spreading of TDP-43 pathology to the contralateral side of the brain of CamKIIa-hTDP-43_{NLSm} mice injected with brain-derived TDP-43 from human brains of different FTLD-TDP subtypes

Fig. S8 Heat-map of regions affected with TDP-43 pathology burden by region and time point post-injection

Fig. S9 TDP-43 pathology induced in the brain of CamKIIa-hTDP-43_{NLSm} mice injected with brain-derived TDP-43 type C and type E extracts at 9 mpi

Supplementary Tables

Table S1 Genetic and demographic data of the human FTLD-TDP cases used in this study

Table S2 ELISA analysis of TDP-43 protein content and BCA measures in sark-insoluble extracts from FTLD-TDP cases used *in vitro* and *in vivo*

Table S3 Sark-insoluble extracts used *in vivo* and the number of CamKIIa-hTDP-43_{NLSm} mice used in each time point

Table S4 Antibodies used in this study

Table S5 Identification of brain areas represented in the heat map analysis

Supplementary references

Supplementary methods

Cytotoxicity and viability assay

iGFP-NLSm cells were plated on PDL (poly-D-lysine, Sigma-Aldrich, #P0899) coated 96-well plates (Perkin Elmer, #50–905–1605) with a density of 6.0×10^3 cell/well. Cells were transduced with ~ 0.20-0.25 µg of brain-derived FTLD-TDP extracts containing ~60-80 pg of TDP-43/well. Bioporter alone and a non-pathological case (CTRL) were used as control. Three days post-transduction both LDH (Pierce™ LDH Cytotoxicity Assay Kit, #88953) and Alamar blue assays (alamarBlue™ Cell Viability Reagent, Invitrogen, #DAL1025) were performed following the manufacturer's instructions.

Live cell-imaging

Live cell-imaging analysis was performed in iGFP-NLSm cells plated in poly-D-lysine coated (100 µg/ml, P0899, Millipore Sigma, St. Louis, MO) MatTek dishes with glass coverlips (35mm, #P35G-1.5-7-C, MatTek Corporation, Ashland, MA). After transduction, the culture dish was secured inside a moist chamber maintained at 37 °C in humidified atmosphere containing 5% CO_2. After two days of transduction, 40X fields containing cells bearing incipietnt GFP-NLS cytoplasmic aggregates were selected. Time-lapse images were taken every 30 min for additional 24h in a high-resolution Leica DMI6000B microscope using the Leica LAS-X software.

Enzyme-linked Immunosorbent Sandwich Assay (ELISA)

The TDP-43 concentrations in the sarkosyl-insoluble fractions were estimated using the 384-well format sandwich ELISA as previously described [1, 6]. Briefly, CNDR mAb 205 was used as a capture antibody (Table S4). Full-length recombinant TDP-43 protein standards (0-10 ng/ml) and sark-insoluble human brain extracts were added to the wells and incubated for 16 h at 4 °C. Plates were washed and incubated with a rabbit polyclonal antibody against C-terminus TDP-43 (C2089) or N-terminus TDP-43 (N1065) (Table S4) for 16 h at 4 °C. Horse-radish peroxidase conjugated goat anti-rabbit IgG and TMB peroxidase was the substrate system (Thermo Scientific Inc., Rockford, IL) used for reporting.

Immunodepletion (ID) and Immunoprecipitation (IP) of TDP-43 from FTLD-TDP extracts

Twenty µl of Dynabeads® Protein G beads (Thermo Scientific Inc., Rockford, IL) were conjugated with 5 µg of anti-TDP-43 antibody (C2089) or control purified rabbit IgG (2729S, Cell Signaling Technology, Inc., Danvers, MA) following the manufacturer's instructions. Thirty µg of sark-insoluble FTLD-TDP extracts (0.3 µg protein/µl) were incubated with either control IgG or C2089 antibodies coupled to beads overnight at 4 °C. The unbound fraction was separated from the antibody/beads complex using a magnet and the immunodepletion was validated by immunoblot. The bound fraction was incubated 30 min at 37°C with 100 µl of HS buffer containing 2% sarkosyl as detergent [1] and sonicated briefly,the remaining bound material was

removed using a magnet. The immunoprecipitated material (IP) was centrifuged 100,000xg for 30 min at 4 °C and pellet resuspended in PBS.

Heat-map

For quantification of TDP-43 pathology (p409-410 positive staining), coronal sections were selected to closely match the following coordinates, relative to bregma; -2.3, −3.52 mm and −4.48 mm (3 sections/ bregma/mouse). The digitised images were imported into HALO software to allow annotation and quantification of the percentage area occupied by TDP-43 pathology [2]. Standardised annotations were drawn to allow independent quantification of 74 regions containing cortical and hippocampal areas throughout the brain [3]. Brain regions were marked according to the anatomical patterns in The Mouse Brain Atlas in stereotaxic coordinates [4]. After annotation of all brain sections, analysis algorithms were applied to all stained sections to detect p409-410 positive staining and data analysis measures for each region were recorded. Data was normalised and transformed to a scale color of 0-3. After grading individual brain regions for each brain sections, mean values of percentage area occupied by TDP-43 pathology in mice injected with different FTLD-TDP subtypes; type A, B and E and the different time point analysed (1 mpi (type A, type B, type E, n=3 mice/group) and 3 mpi (type A, type B, type E, n=3 mice/group)) were used to generate heat maps using the in-house software to graphically show distribution of TDP-43 pathology based on a scale-color system [5]. The percentage area occupied by TDP-43 pathology in each brain region and for each individual injected mouse was represented as a heat-map plots using the Graph Pad 7.0 software.

Supplementary Figures

Figure S1

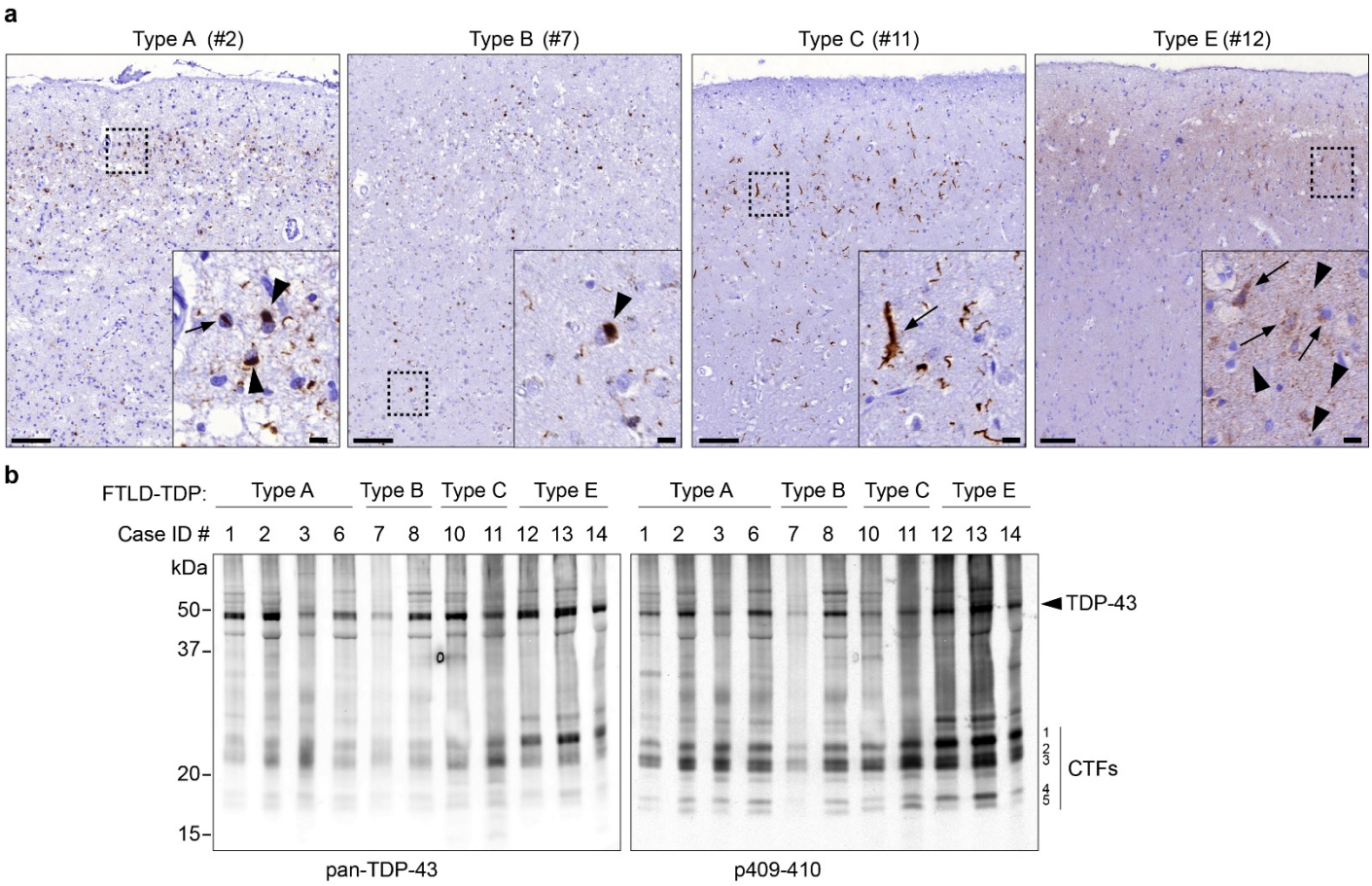

Fig. S1 Differential neuropathological distribution of phosphorylated TDP-43 aggregates and biochemical analysis of sark-insoluble brain extracts from different FTDP-TDP subtypes used in this study

a) Representative photomicrographs of p409-410 immunostaining in frontal cortex sections of different FTLD-TDP subtypes (A, B, C and E). Cases are identified by numbers corresponding to those in Table S1 (Case ID #). Insets show characteristic neuropathological features of each FTLD-TDP subtype. Type A comprise neuronal cytoplasmic inclusions (NCIs, inset arrowheads), neuronal intranuclear inclusions (NII, inset arrow), and abundant short dystrophic neurites (DNs) in superficial layers while type B, NCIs are in superficial and deep layers (inset, arrowhead) and type C are long thick ropy DNs (inset arrow), moreover type E are granulofilamentous neuronal inclusions (GFNIs, inset arrows) and neuropile grains (inset arrowhead). Scale bar= 100 μm; insets=10 μm. b) Immunoblot analysis of the sark-insoluble fractions from the frontal cortex of different FTLD-TDP subtypes using a pan-TDP-43 antibody (C2089) and a phosphorylation-specific TDP-43 specific antibody (p409-410). Brains extracts representing each FTLD-TDP subtype are identified by numbers corresponding to those in Table S1 (Case ID #). Molecular weight markers in kDa are shown on the left and the position of full-length TDP-43 protein (arrowhead) and C-terminal fragments CTFs (bands #1, #2, #3, #4 and #5) on the right.

Figure S2

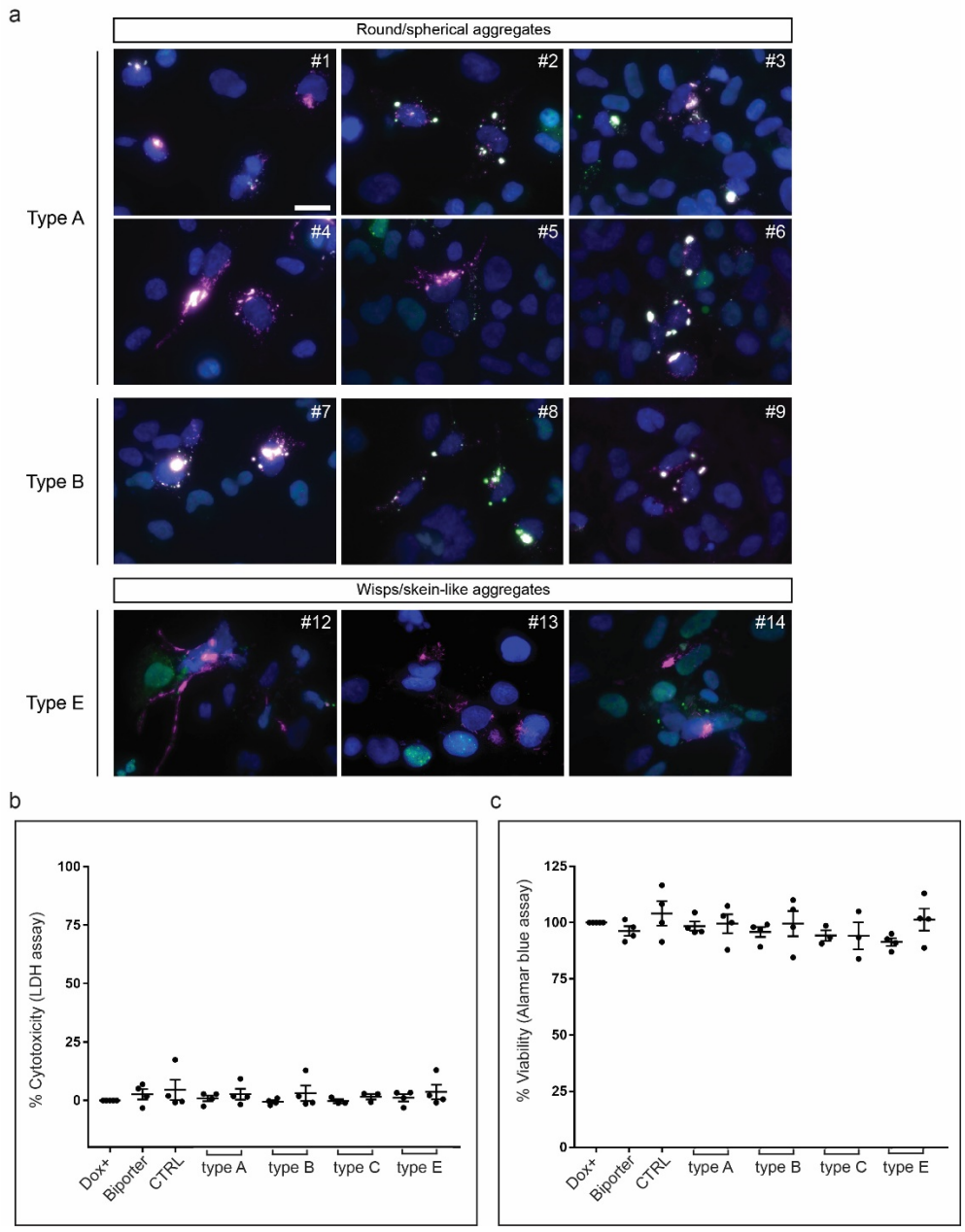

Fig. S2 Morphological differences of TDP-43 aggregates in iGFP-NLSm cells transduced with distinct FTLD-TDP subtypes are not associated with differences in cytotoxicity or cell viability

Representative ICC images of GFP-NLSm expressing cells (green) transduced with sark-insoluble brain extracts from different FTLD-TDP subtypes at 3 days post-transduction (dpt) showing 1% Triton-insoluble phospho-TDP-43 positive cytoplasmic aggregates (magenta). Top panels show characteristic round/spherical aggregates induced when type A and type B brain extracts are used as seeds. Bottom panels show characteristics wisps and skein-like aggregates induced by type E seeds. FTLD-TDP cases are identified by numbers (#) corresponding to those in Table S1 (Case ID #). Cells were counterstained with DAPI to label the nuclei (blue). Scale bar=20 µm. Cytotoxicity and cell viability were measured at 3 dpt using LDH (**b**) and Alamar Blue (**c**) assay, respectively. Plots show the percentage of cytotoxicity (a), and viability (b) in cells transduced with either Bioporter alone, a brain-extract from a non-pathological case (CTRL), or different FTLD-TDP subtypes (type A, B, C and E (n=2 cases/type)) respect non-transduced conditions (Dox+). Data show the mean ± SEM, with individual points representing different experiments (n=3-4). For each experiment, LDH and Alamar Blue assays were analysed in five different wells per condition.

Figure S3

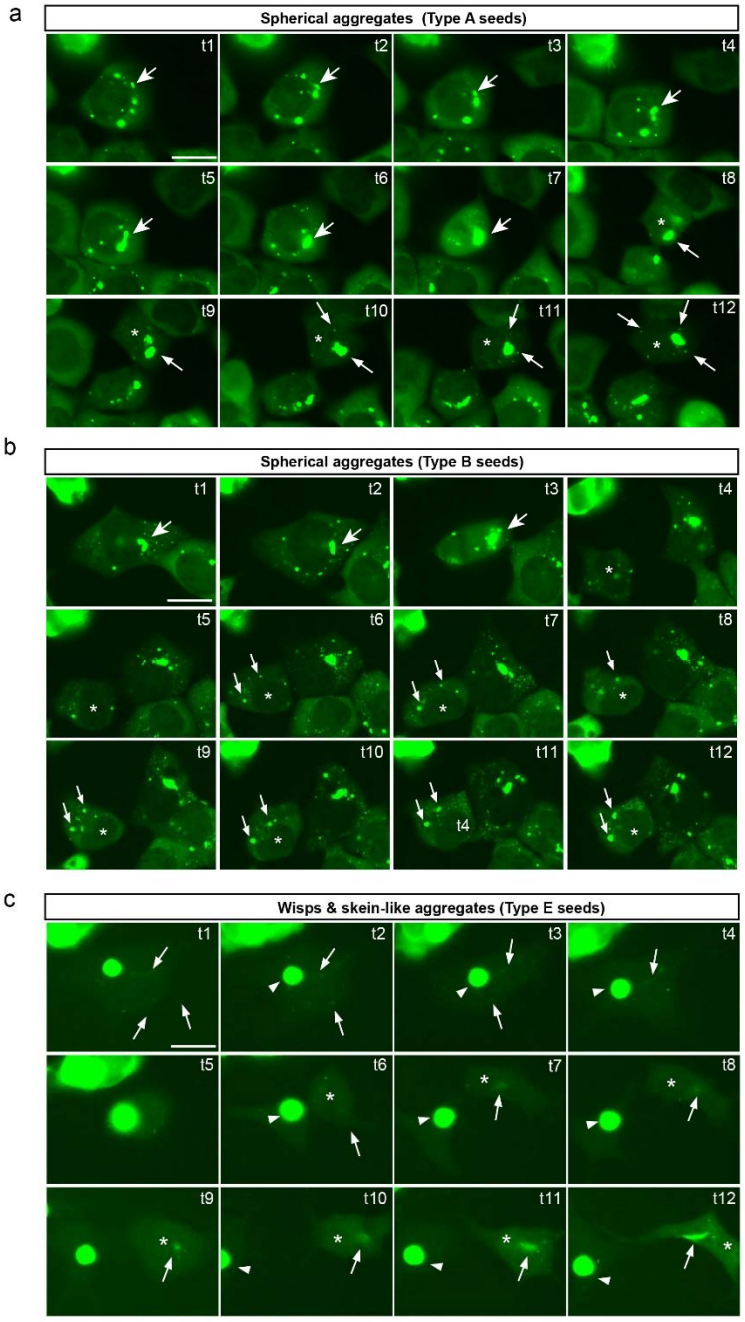

Fig. S3 Morphological features of TDP-43 aggregates induced in iGFP-NLSm cells are propagated from progenitor to offspring cells

Time-lapses of live-cell imaging of iGFP-TDP-43$_{NLSm}$ transduced with type A and B seeds bearing spherical aggregates (a and b, respectively) and wisps and skein-like aggregates in cells transduced with type E seeds (c). Images show a 12-hrs time-frame (t1-t12) of a total of 24 hrs of recording live iGFP-NLSm cells from day 2 to day 3 post-transduction (see movies 3, 4 and 5). a and b) Arrows point to cytoplasmic spherical and more elongated GFP-NLSm aggregates and asterisks mark the offspring cells. c) Arrows point to wisps and arrowheads to skein-like aggregates. In c to distinguish the wisps from the cytoplasmic GFP-NLSm expression, the fluorescence signal was overexposed, and consequently, the skein-like aggregates appear like big blobs. Asterisks mark the offspring cells. Scale bar=20 μm (a, b and c).

Figure S4

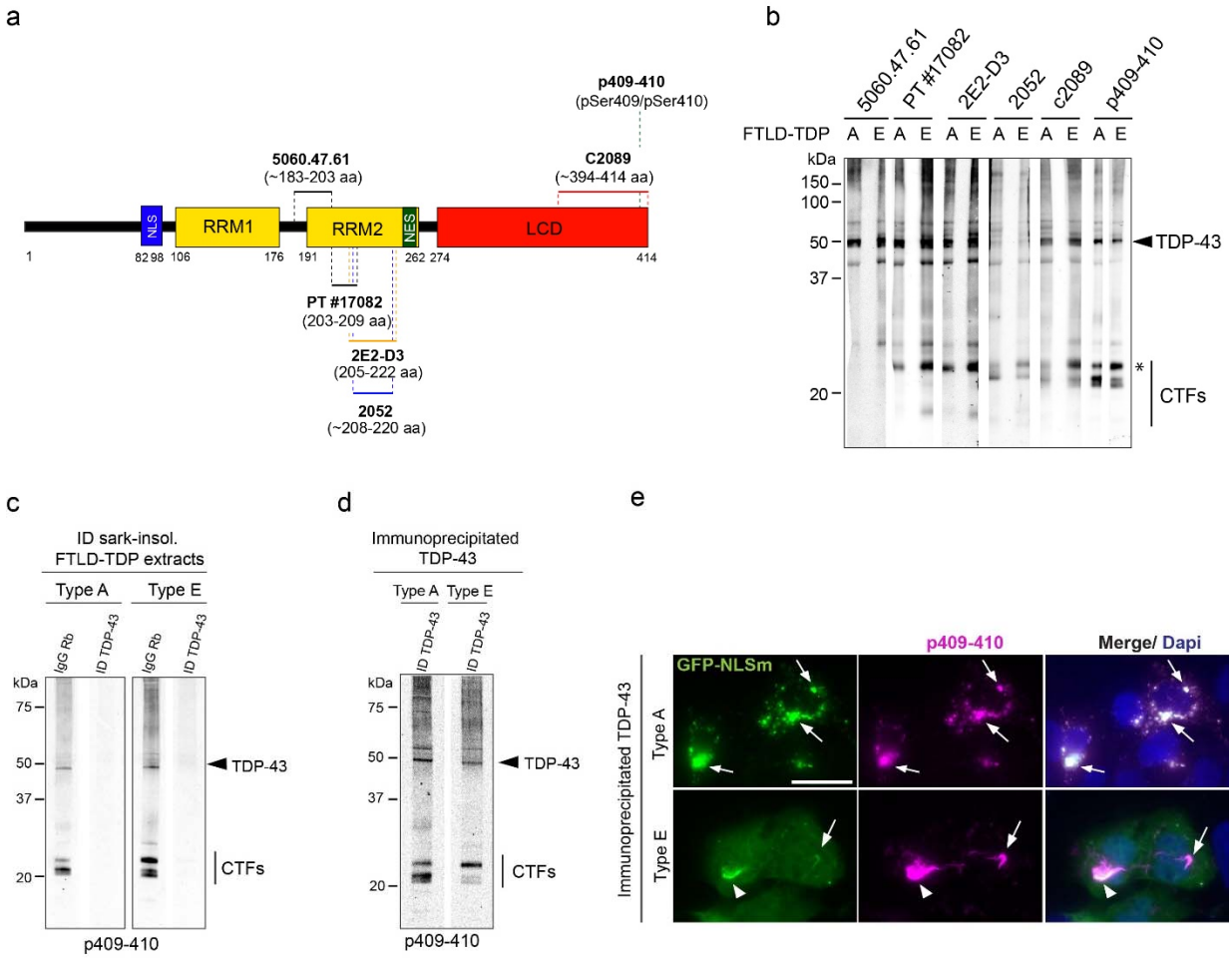

Fig. S4 Differences in morphological features of TDP-43 aggregates are associated with distinct TDP-43 strains in different FTLD-TDP subtypes

a) The schematic diagram illustrates the epitopes recognised by specific antibodies against TDP-43 protein. Colored boxes represent TDP-43 domains as follows: nuclear localization signal (NLS, blue), RNA recognition-motifs 1 and 2 (RRM1 and RRM2, yellow), nuclear export signal (NES, green) and the low complexity domain (LCD, red). b) Immunoblot analysis of the sark-insoluble fraction from FTLD-TDP brain extracts. Note that types A and E extracts are in separate lanes and that different anti-TDP-43 antibodies were used as illustrated in a. Molecular weight markers in kDa are shown on the left, and the position of the full-length TDP-43 protein (arrowhead) and the characteristic C-terminal fragments (CTFs) are located on the right. The asterisk in the top right panel marks the top CTF band that is more prominent relative to the other CTFs in type E extracts. c) Images show immunoblot analysis of unbound proteins in the sark-insoluble fraction from FTLD-TDP brain extracts as shown in lanes identified as type A and type E after immunodepletion (ID) with a rabbit polyclonal antibody against TDP-43 (lanes ID TDP43) or rabbit IgGs as a control (lanes IgG Rb). The membranes were immunoblotted with the p409-410 antibody. Molecular weight markers in kDa are shown on the left, and the position of the full-length TDP-43 protein (arrowhead) and the characteristic C-terminal fragments (CTFs) are located on the right. d) Image shows immunoblot analysis of the immunoprecipitated TDP-43 proteins from sark-insoluble FTLD-TDP brain extracts (lanes type A and type E) e) ICC images show p409-410 positive aggregates (magenta and merge) in GFP-NLSm expressing cells (green and merge) transduced with the immunoprecipitated TDP-43 protein from type A and type E extracts (ID TDP-43 in d) at 3 dpt. Arrows point to cytoplasmic spherical aggregates (top panels) and wisps (bottom panels), and arrowheads point to skein-like aggregates (bottom panels). Cells were counterstained with DAPI to label the nuclei (blue). Scale bar = 20 μm.

Figure S5

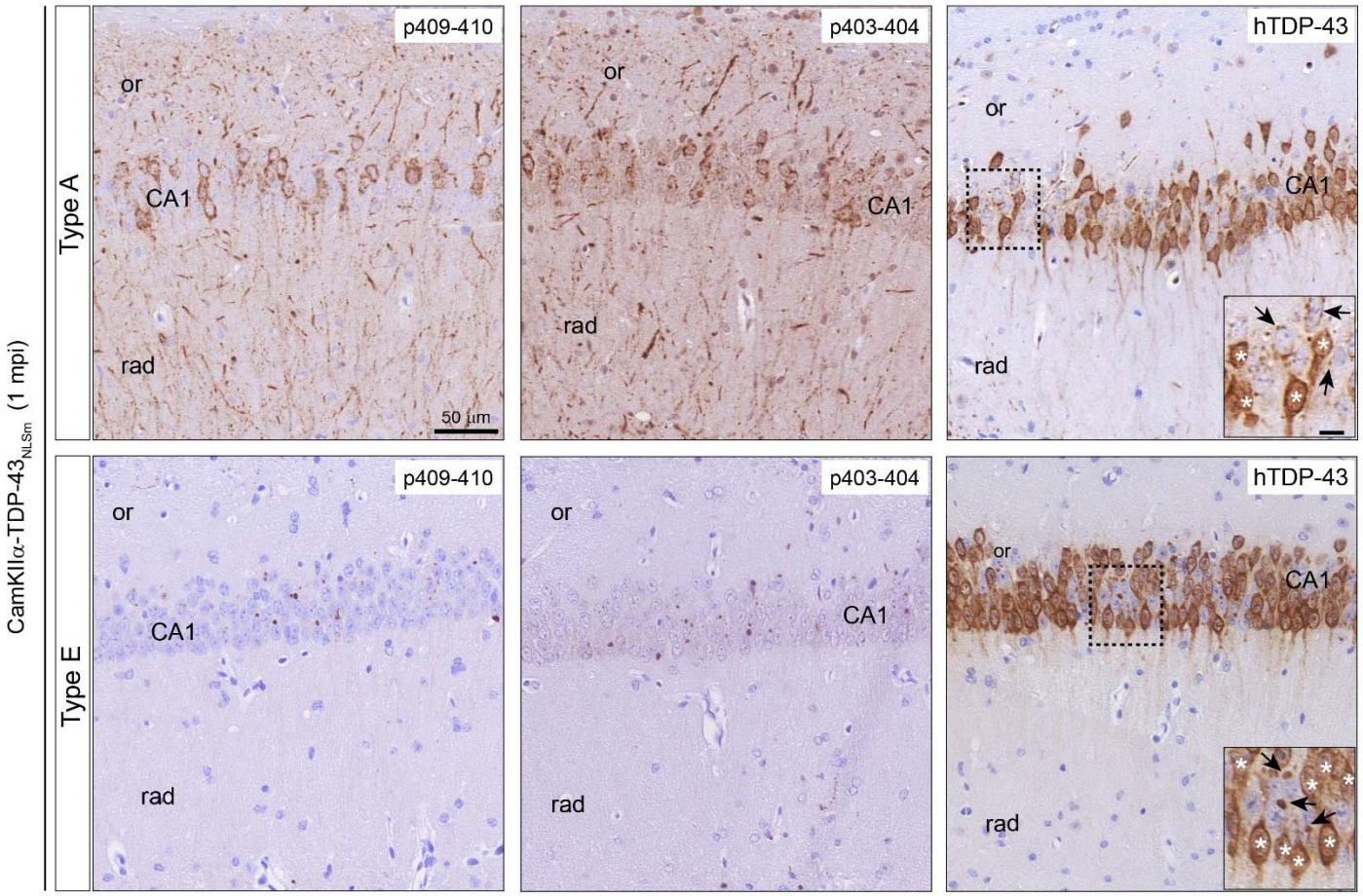

Fig. S5 TDP-43 aggregates are phosphorylated at Ser409/Ser410 and Ser403/Ser404 residues and cytoplasmic hTDP-43$_{NLSm}$ proteins entirely recruited into inclusions.

Representative photomicrographs of immunohistochemical staining in the hippocampus of CamKIIa-hTDP-43$_{NLSm}$ mice injected with sark-insoluble extracts from type A (top panels) and type E (bottom panels) cases at 1 mpi. Coronal brain sections were immunostained using the phospho-specific antibodies; p409-410 (left panels) or p403-404 (middle panels), and a polyclonal antibody that preferentially recognizes exogenous hTDP-43 protein (right panels). Images show p409-410-immunopositive aggregates as well as p403-404 immuno-positive staining in the CA1 layer of the hippocampus with its projection areas such as stratum radiatum (rad), and oriens (or) in mice injected with type A extracts. Images from mice injected with type E extracts show p409-410 and p403-404 positive dot-like aggregates in CA1 layer. In the left panels, asterisks mark neurons with the characteristic neuronal cytoplasmic distribution of hTDP-43$_{NLSm}$ protein in CamKIIa-hTDP-43$_{NLSm}$ mice. Arrows point to neurons showing hTDP-43$_{NLSm}$ protein recruited into cytoplasmic aggregates. Insets show higher magnifications of the black-dashed boxes. Scale bar=50 μm and 10 μm (insets).

Figure S6

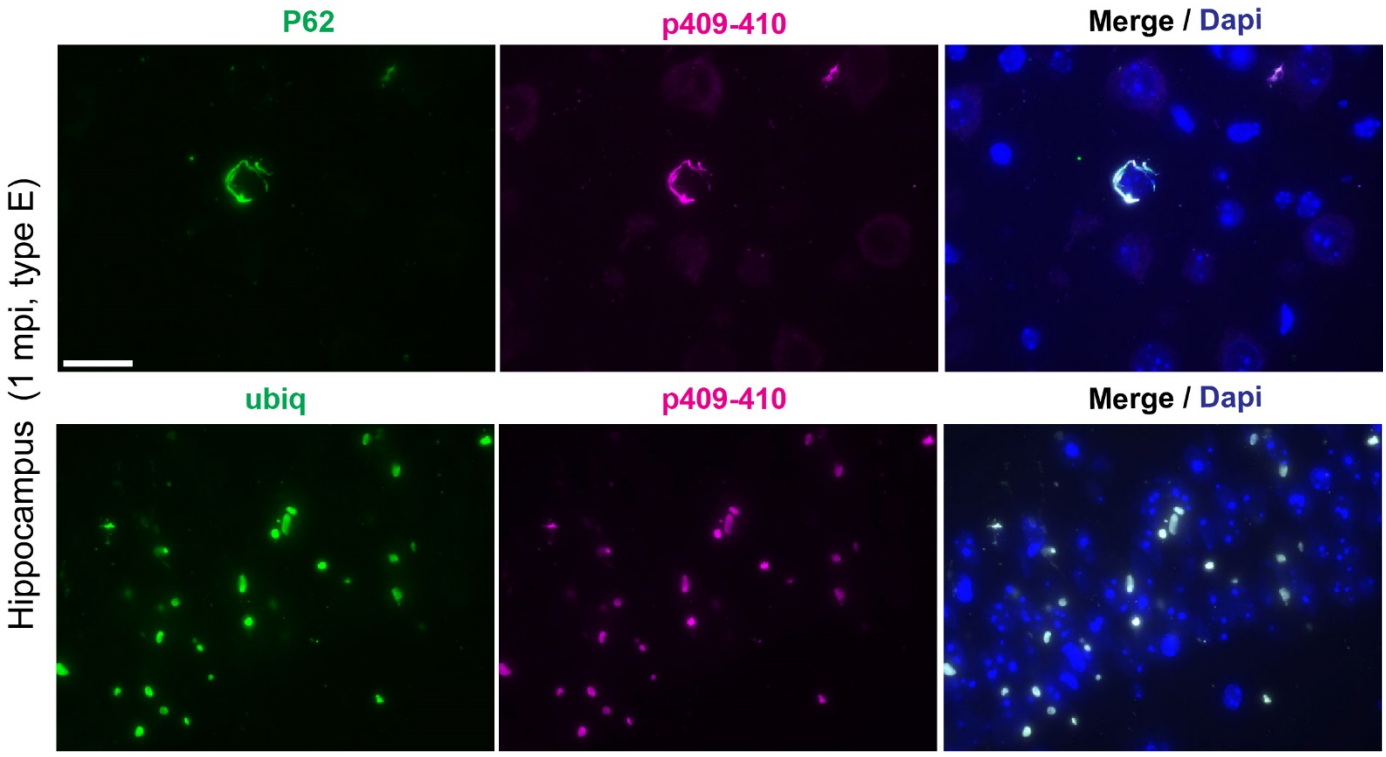

Fig. S6 p409-410 positive NCIs co-localize with p62 and ubiquitin

Representative double-label immunofluorescence (IF) images of p409-410 immunostaining of p409-410 positive NCIs (magenta and merge) and P62 (green and merge) and ubiquitin (green and merge) proteins in the hippocampus of CamKIIa-hTDP-43$_{NLSm}$ mice injected with type E extracts at 1 mpi. Brain sections were counterstained with DAPI to label the nuclei (blue). Scale bar = 20 μm.

Figure S7

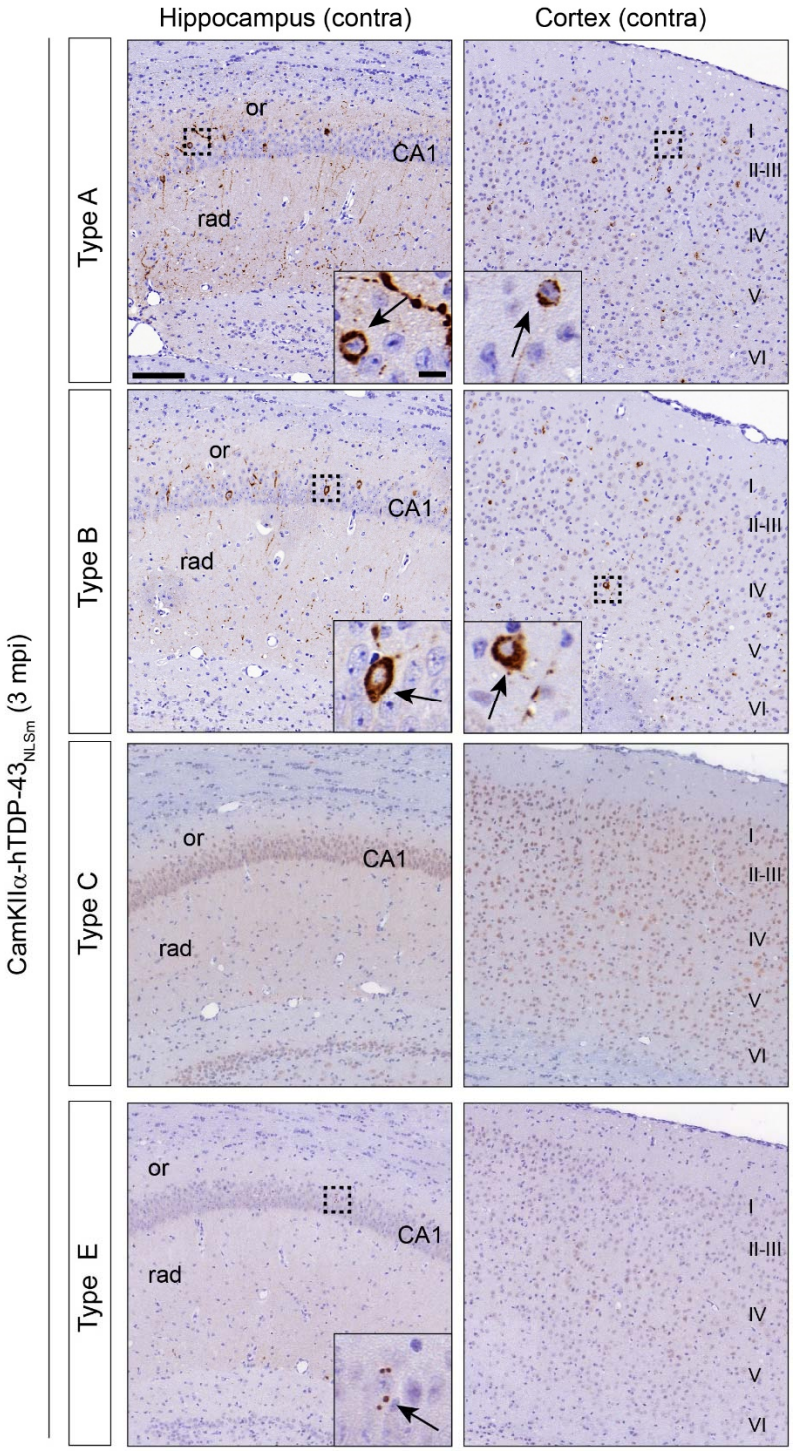

Fig. S7 Spreading of TDP-43 pathology to the contralateral side of the brain of CamKIIa-hTDP-43NLSm mice injected with brain-derived TDP-43 from human FTLD-TDP brains of different subtypes

Representative photomicrographs of p409-410 immunostaining in coronal brain sections at 3 mpi from CamKIIa-hTDP43$_{NLSm}$ mice stereotaxically injected with human brain-derived TDP-43 from different FTLD-TDP subtypes; type A, type B, type C, and type E. Images show p409-410 immunostaining in the contralateral side of the brain (contra) in the hippocampus (cornu amonis (CA1 layer), stratum radiatum (rad), and oriens (or)), and neocortical areas (cortex, layers I–VI). Insets show higher magnifications of the black-dashed boxes. Scale bar=100 µm and 10 µm (insets).

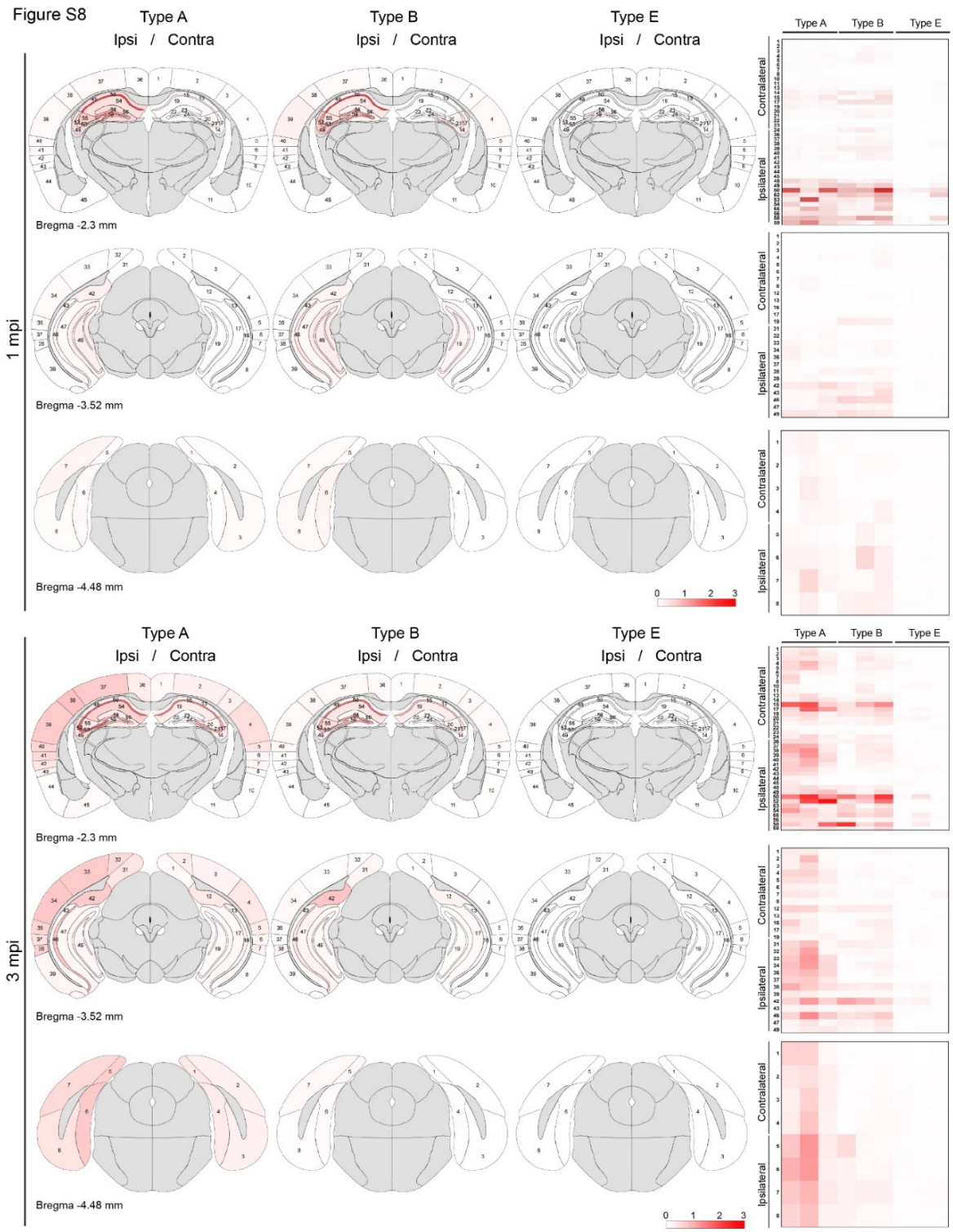

Fig. S8 Heat-map of regions affected with TDP-43 pathology burden by region and time post-injection

The burden of TDP-43 pathology determined as a percentage of area occupied with p409-410 positive immunostaining in three representative coronal sections from CamKIIa-hTDP-43$_{NLSm}$ mice injected with different FTLD-TDP extracts (type A, B and E) and at different time post-injection (1 and 3 mpi). Each panel illustrated here depicting rostral to causal brain regions represents a coronal plane (Bregma; -2.3 mm, -3.52 mm and -4.48 mm). The mean percentage of area occupied with p409-410 positive immunostaining at 1 mpi (type A, type B and type E, n=3 mice/group) and at 3 mpi (type A, type B and type E, n=3 mice/group) was color-coded from negative (0, white) to most abundant (3, red) in each cortical and hippocampal area analysed. The percentage of area occupied with TDP-43 pathology (contralateral and ipsilateral) in each individual injected CamKIIa-hTDP-43$_{NLSm}$ mouse is represented as color-scale plots (right panels). The names of each brain area associated to each number are defined in supplementary Table S5.

Figure S9

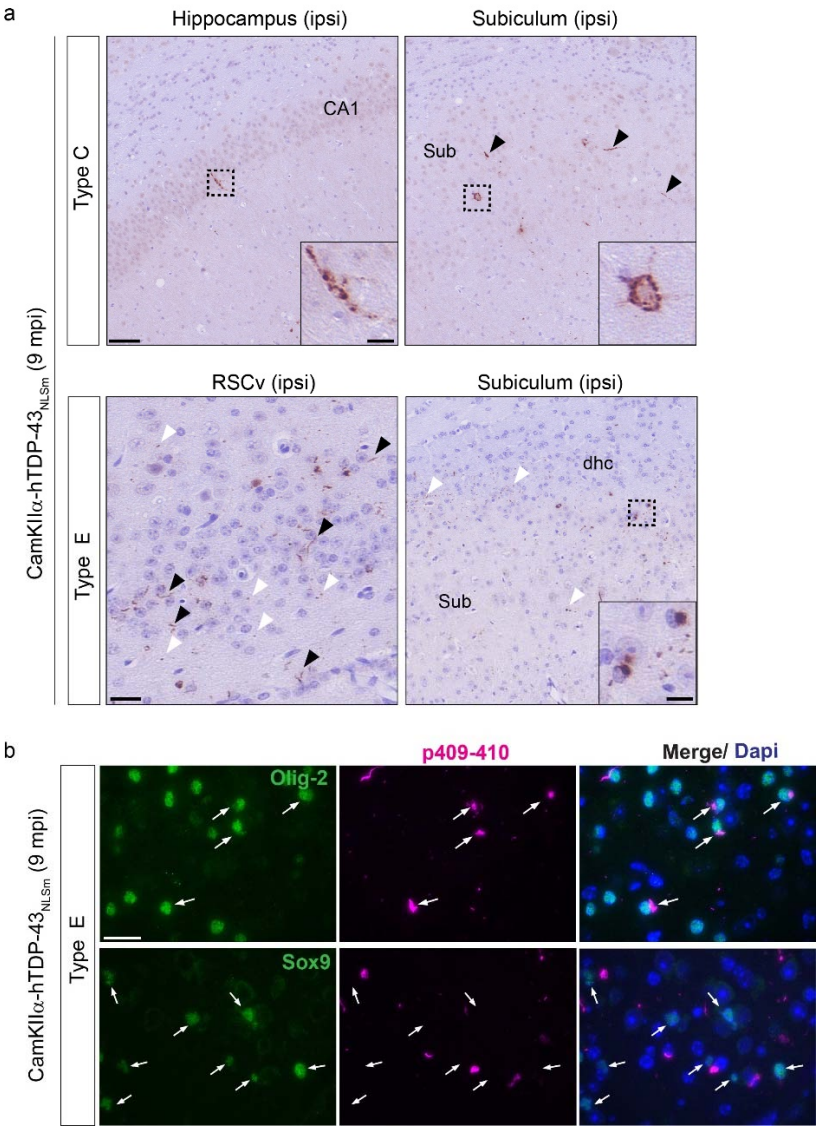

Fig. S9 TDP-43 pathology induced in the brains of CamKIIa-hTDP-43$_{NLSm}$ mice injected with brain-derived TDP-43 from type C and type E extracts at 9 mpi

a) Images of p409-410 immunostaining in coronal brain sections CamKIIa-hTDP43$_{NLSm}$ mice injected with type C and type E extracts at 9 mpi. Top panels show images of the p409-410 positive staining found in one of ten mice injected with type C extracts in the ipsilateral hippocampus (ipsi), in the CA1 and subiculum (sub). Bottom panels show representative images of the p409-410 positive staining in the ipsilateral (ipsi) ventral restrosplenial cortex (RSCv) and subiculum (sub) including the adjacent dorsal hippocampal commissure (dhc) in CamKIIa-hTDP43$_{NLSm}$ mice injected with type E extracts. Black arrowheads point to p409-410 positive threads and white arrowheads point to dotted p409-410 immunostaining in the neuropil. Insets show higher magnifications of the black-dashed boxes. b) Representative fluorescent images of p409-410 immunostaining (magenta and merge) showing oligodendroglia (Olig-2, green and merge) and astrocytes (Sox9, green and merge) in RSCv of CamKIIa-hTDP-43$_{NLSm}$ mice injected with type E extracts at 9 mpi. Brain sections were counterstained with DAPI to label the nuclei (blue). Arrows point to oligodendrocytes bearing p409-410 positive inclusions, however, p409-410 positive staining was largely not associated with Sox9 positive cells (arrowheads). Scale bar= 50 µm (a), 20 µm (b), and 10 µm (insets).

Supplementary Tables

Table S1. Genetic and demographic data of the human FTLD-TDP cases used in this study

Case ID #	Neuropathological Diagnosis	FTLD-TDP subtype *	Genetic mutations	Clinical Phenotype	Gender	Age at onset	Age at death	PMI (hrs)
1	FTLD-TDP	A	-	bvFTD	F	66	74	22
2	FTLD-TDP	A	-	Dementia of undetermined etiology	F	N/A	82	12
3	FTLD-TDP	A	GRN c.154delA, p.T52HfsX2	bvFTD	F	61	69	19
4	FTLD-TDP	A	GRN c.1317_1318delCA, p.Asp441HisfsX4	Corticobasal syndrome	M	50	55	23
5	FTLD-TDP	A	GRN c.675_676delCA, p.Ser226TrpfsX28	aPPA	M	56	66	18
6	FTLD-TDP	A	C9orf72 Expansion	bvFTD	M	53	60	21
7	FTLD-TDP	B	-	PPA (naPPA/)	F	67	73	11
8	FTLD-TDP	B	C9orf72 Expansion	Probable Alzheimer's Disease	M	71	77	5
9	FTLD-TDP	B	C9orf72 Expansion	FTLD-NOS	M	70	75	10
10	FTLD-TDP	C	-	Probable Alzheimer's Disease	M	68	79	5
11	FTLD-TDP	C	-	PPA (naPPA/svPPA)	M	NA	63	12.5
12 #	FTLD-TDP	E	-	bvFTD	M	62	65	6
13 #	FTLD-TDP	E	-	bvFTD	F	58	61	18
14	FTLD-TDP	E	C9orf72 Expansion	bvFTD	F	66	72	5
15	CTRL	-	-	-	F	-	60	9

* Classification system (Mackenzie et al. 2011, Mackenzie et al. 2017 and Lee et al. 2017)

FTLD-TDP type E cases characterised in Lee et al. 2017

Abbreviations: bvFTD - behavioral variant frontotemporal degeneration, PPA - Primary progressive aphasia, naPPA - non-fluent/agrammatic variant of PPA, svPPAsemanticvariant of PPA, N/A - not available, PMI – post mortem interval

Table S2. ELISA analysis of TDP-43 protein content and BCA measures in sark-insoluble extracts from FTLD-TDP cases used *in vitro* and *in vivo*.

Case ID #	Neuropathological Diagnosis	FTLD-TDP subtype *	ELISA C89** (ng TDP-43/ml)	ELISA N65** (ng TDP-43/ml)	BCA (mg/ml)	TDP-43 (Elisa c89)**/total protein TDP-43 (Elisa N65)**/total protein (%)
1	FTLD-TDP	A	310	289	2.30	0.013-0.013
2	FTLD-TDP	A	451	346	3.40	0.013-0.010
3	FTLD-TDP	A	791	855	4.80	0.016-0.018
4	FTLD-TDP	A	741	314	3.90	0.019-0.008
5	FTLD-TDP	A	520	321	2.60	0.020-0.012
6	FTLD-TDP	A	277	205	1.40	0.020-0.015
7	FTLD-TDP	B	1,411	1,165	4.57	0.031-0.025
8	FTLD-TDP	B	846	507	3.91	0.022-0.013
9	FTLD-TDP	B	310	118	3.60	0.009-0.003
10	FTLD-TDP	C	608	356	3.49	0.017-0.010
11	FTLD-TDP	C	558	391	5.03	0.011-0.008
12 #	FTLD-TDP	E	1,337	685	3.76	0.036-0.018
13 #	FTLD-TDP	E	919	344	2.59	0.036-0.013
14	FTLD-TDP	E	608	460	4.30	0.014-0.011
15	CTRL	-	63	43	2.10	0.003-0.002

* Classification system (Mackenzie et al. 2011, Mackenzie et al. 2017 and Lee et al. 2017)

** ELISA measure of TDP-43 content using a C-terminus (C89) or N-terminal (N65) anti-TDP-43 antibody as a reporter

FTLD-TDP type E cases characterised by Lee et al. 2017

Table S3. Sark-insoluble extracts used *in vivo* and the number of CamKIIa-hTDP-43$_{NLSm}$ mice used in each time point

Case ID #	FTLD-TDP subtype *	Genetics	1 mpi	3 mpi	9 mpi
2	A	-	n=3	n=4	N/A
3	A	GRN	n=6	n=3	**
7	B	-	n=2	n=2	N/A
8	B	C9+	n=3	n=3	N/A
10	C		n=2	n=2	n=2
11	C		n=2	N/A	n=3
12 #	E		n=5	n=4	n=2
13 #	E		n=2	n=3	N/A
14	E		n=2	n=3	N/A

* Classification system (Mackenzie et al. 2011, Mackenzie et al. 2017 and Lee et al. 2017)

** Time point previously tested in vivo and described in Porta et al., 2018

FTLD-TDP type E cases characterised in Lee et al. 2017

Abbreviations: mpi- months post injection, N/A – not assessed

Table S4. Antibodies used in this study

Name antibody	Epitope	Source (Cat. #)	Host	Method (dilution or concentration (µg/ml)			
				IHC	ICC	IB	ELISA
5104 mass	human TDP-43 (aa 261-393)	In-house [6]	Mo (IgG1)	0.017		0.17	
N1065	TDP-43 (aa 6-24)	In-house [7]	Rb				1.0
205.25.26	TDP-43 (aa 261-393)	In-house [6]	Mo (IgG2a)				5.0
C1039	TDP-43 (aa 394-414)	In-house [8]	Rb			0.03	
C2089	TDP-43 (aa 394-414)	In-house	Rb			0.10	0.10
5060.47.61	TDP-43 (aa 183-203)	In-house	Mo (IgG2a)			5.0	
PT #17082	TDP-43 (aa 203-209aa)	Proteintech (17082-2-AP)	Rb			0.25	
2E2-D3	human TDP-43 (aa 205-222)	Abnova (H00023435-M01)	Mo (IgG1)			1.0	
2052	TDP-43 (aa 208-220)	In-house [8]	Rb serum			1:500	
p409-410	pTDP-43 (phosphorylated at Ser409/Ser410)	Ascenion, Munich (Germany) (TAR5P-1D3) [9]	Rat	1:200	1:200	1:200	
p409-410	pTDP-43 (phosphorylated at Ser409/Ser410)	Cosmo Bio Co., Ltd. (CAC-TIP-PTD-P01)	Rb	1:10,000			
p403-404	pTDP-43 (phosphorylated at Ser403/Ser404)	Cosmo Bio Co., Ltd. (CAC-TIP-PTD-P05)	Rb	1:3,000			
P62	SQSTM1 (sequestosome 1)	Abnova (H00008878-M01)	Mo (IgG2a)	1:500			
Ubiq	ubiquitin	Millipore (MAB1510)	Mo (IgG1)	1:3,000			
Olig2	Olig2 (oligodendroglia)	Millipore (9610)	Rb	1:250			
Sox9	Sox9 (astroglia)	Abcam	Rb	1:500			
Biotinilated anti-rat IgG (H+L)		Vector (BA-4001)	Rb	1:300			
Biotinilated anti-rabbit IgG (H+L)		Vector (BA-1000)	Goat	1:1,000			
anti-rabbit IRDye 680RD		LI-COR Bioscience (926-68071)	Goat			1:20,000	
anti-mouse IgG IRDye 680RD		LI-COR Bioscience (926-32210)	Goat			1:20,000	
anti-rat IRDye 800RD		Rockland (612-132-120)	Goat			1:10,000	
anti-rat IRDye 680RD		LI-COR Bioscience (926-68076)	Goat			1:10,000	
anti-mouse IRDye 800RD		LI-COR Bioscience (926-32210)	Goat			1:20,000	
anti-rabbit IgG IRDye 800CW		LI-COR Bioscience (926-32211)	Goat			1:20,000	
anti-rabbit Alexa Fluor 594-conjugated		Molecular Probes	Goat	1:1,000	1:1,000		
anti-rat Alexa Fluor 594-conjugated		Molecular Probes	Goat	1:1,000	1:1,000		
anti-mouse Alexa, Fluor 488-conjugated		Molecular Probes	Goat	1:1,000	1:1,000		
anti-rabbit Alexa, Fluor 488-conjugated		Molecular Probes	Goat	1:1,000	1:1,000		

Abbreviations; IHC – immunohistochemistry, ICC - immucytochemistry, IB - immunoblot; ELISA – Enzyme Linked Immunosorbent Sandwich Assay

Table S5. Identification of brain areas associated to numbers in the heat-map analysis

	Brain area #ID			
	Ipsilateral	**Contralateral**	**Abbreviations**	**Full name**
Bregma -2.3 mm	36	1	RSG/RSA	retrosplenial granular cortex/retrosplenial agranular cortex
	37	2	V2MM/V2ML/V1/V2L	secondary visual cortex, mediomedial area/secondary visual cortex, mediolateral area/primary visual cortex/secondary visual cortex, lateral area
	38	3	S1	primary somatosensory cortex
	39	4	AuD/Au1/AuV	secondary auditory cortex, dorsal area/primary auditory cortex /secondary auditory cortex, ventral area
	40	5	TeA	temporal association cortex
	41	6	Ect	ectorhinal cortex
	42	7	PRh	ectorhinal cortex
	43	8	Lent	lateral entorhinal cortex
	44	10	Pir	piriform cortex
	45	11	PLCo-PMCo, AHiAL,DG	postero lateral and medial cortical amygdaloid nucleus, amygdalohippocampal area (anterolateral part), dentate gyrus
	48	13	Or	oriens layer of the hippocampus
	49	14	Or ventral part	oriens layer of the hippocampus (ventral part)
	50	15	CA1, CA2	CA1 and CA2 pyramidal cell layer of the hippocampus
	52	17	CA3	CA3 pyramidal cell layer of the hippocampus
	53	19	Slu	stratum lucidum, hippocampus
	54	20	Rad/LMol	stratum radiatum of the hippocampus/lacunosum moleculare layer of the hippocampus
	55	21	Rad/Lmol ventral part	stratum radiatum of the hippocampus/lacunosum moleculare layer of the hippocampus (ventral part)
	56	22	DG	dentate gyrus
	58	23	GrDG	granular layer of the dentate gyrus
	59	24	PoDG	polymorph layer of the dentate gyrus
Bregma -3.52 mm	31	1	RSG	retrosplenial granular cortex
	32	2	RSA/V2MM/V2ML	retrosplenial agranular cortex/secondary visual cortex, mediomedial area/secondary visual cortex, mediolateral area
	33	3	V1/V2L	primary visual cortex/secondary visual cortex, lateral area
	34	4	AuD/Au1	secondary auditory cortex, dorsal area/primary auditory cortex
	36	5	TeA	temporal association cortex
	37	6	Ect	ectorhinal cortex
	38	7	PRh	ectorhinal cortex
	39	8	Lent	lateral entorhinal cortex
	42	12	S/PrS	subiculum/presubiculum
	43	13	Or	oriens layer of the hippocampus
	46	16	Rad	stratum radiatum of the hippocampus
	47	17	LMol	lacunosum moleculare layer of the hippocampus
	49	19	GrDG	granular layer of the dentate gyrus
Bregma - 4.48 mm	11	1	RSA	retrosplenial agranular cortex
	12	2	V2MM/V1/V2L/TeA/Ect	secondary visual cortex, mediomedial area/primary visual cortex/secondary visual cortex, lateral area/temporal association cortex /ectorhinal cortex
	13	3	PRh/Lent/Ment	ectorhinal cortex/lateral entorhinal cortex /medial entorhinal cortex
	14	4	PrS/PaS	presubiculum/parasubiculum

Supplementary References

1 Porta S, Xu Y, Restrepo CR, Kwong LK, Zhang B, Brown HJ, et al. Patient-derived frontotemporal lobar degeneration brain extracts induce formation and spreading of TDP-43 pathology in vivo. Nat Commun 2018; 9: 4220-35

2 Irwin DJ, Byrne MD, McMillan CT, Cooper F, Arnold SE, Lee EB, et al. Semi-Automated Digital Image Analysis of Pick's Disease and TDP-43 Proteinopathy. J Histochem Cytochem 2016; 64: 54-66

3 Henderson MX, Cornblath EJ, Darwich A, Zhang B, Brown H, Gathagan RJ, et al. Spread of alpha-synuclein pathology through the brain connectome is modulated by selective vulnerability and predicted by network analysis. Nat Neurosci 2019; 22: 1248-57

4 Paxinos G, Franklin KBJ. The Mouse Brain in Stereotaxic Coordinates. Second ed. Academic Press, San Diego. 2001

5 Iba M, Guo JL, McBride JD, Zhang B, Trojanowski JQ, Lee VM. Synthetic tau fibrils mediate transmission of neurofibrillary tangles in a transgenic mouse model of Alzheimer's-like tauopathy. J Neurosci 2013; 33: 1024-37

6 Kwong LK, Irwin DJ, Walker AK, Xu Y, Riddle DM, Trojanowski JQ, et al. Novel monoclonal antibodies to normal and pathologically altered human TDP-43 proteins. Acta Neuropathol Commun 2014; 2: 33

7 Walker AK, Spiller KJ, Ge G, Zheng A, Xu Y, Zhou M, et al. Functional recovery in new mouse models of ALS/FTLD after clearance of pathological cytoplasmic TDP-43. Acta Neuropathol 2015a; 130: 643-60

8 Walker AK, Tripathy K, Restrepo CR, Ge G, Xu Y, Kwong LK, et al. An insoluble frontotemporal lobar degeneration-associated TDP-43 C-terminal fragment causes neurodegeneration and hippocampus pathology in transgenic mice. Hum Mol Genet 2015b; 24: 7241-54

9 Neumann M, Kwong LK, Lee EB, Kremmer E, Flatley A, Xu Y, et al. Phosphorylation of S409/410 of TDP-43 is a consistent feature in all sporadic and familial forms of TDP-43 proteinopathies. Acta Neuropathol 2009; 117: 137-49